Discrete element analysis for the assessment of the accuracy of load cell-based dynamic weighing systems in grape harvesters under different ground conditions

C. González-Montellano , E.M. Baguena , Á. Ramírez-Gómez , P. Barreiro

Keywords:
Dynamic weighing
Harvester
Load cell
Discrete element method

A B S T R A C T

Dynamic weighing systems based on load cells are commonly used to estimate crop yields in the field. There is lack of data, however, regarding the accuracy of such weighing systems mounted on harvesting machinery, especially on that used to collect high value crops such as fruits and vegetables. Certainly, dynamic weighing systems mounted on the bins of grape harvesters are affected by the displacement of the load inside the bin when moving over terrain of changing topography. In this work, the load that would be registered in a grape harvester bin by a dynamic weighing system based on the use of a load cell was inferred by using the discrete element method (DEM). DEM is a numerical technique capable of accurately describing the behaviour of granular materials under dynamic situations and it has been proven to provide successful predictions in many different scenarios. In this work, different DEM models of a grape harvester bin were developed contemplating different influencing factors. Results obtained from these models were used to infer the output given by the load cell of a real bin. The mass detected by the load cell when the bin was inclined depended strongly on the distribution of the load within the bin, but was underestimated in all scenarios. The distribution of the load was found to be dependent on the inclination of the bin caused by the topography of the terrain, but also by the history of inclination (inclination rate, presence of static periods, etc.) since the effect of the inertia of the particles (i.e., representing the grapes) was not negligible. Some recommendations are given to try to improve the accuracy of crop load measurement in the field.

1. Introduction

In the 1990s, a number of authors studied the use of grain mass flow sensors in combine harvesters (normally placed at the top of the grain elevator) as a means of generating yield maps (Colvin et al., 1991; Stafford et al., 1991; Vansichen and De Baerdemaeker, 1991). The production of such maps requires the interpolation of instantaneous grain yields in order to estimate the average for a given area (Birrell et al., 1996). Unfortunately, the sensors used in combine harvesters are usually unsuitable for use with other types of crop. Indeed, very few yield monitoring systems are commercially available for use with fruits and vegetables (Durrence et al, 1999; Pelletier and Upadhyaya, 1999; Magalhães and Cerri, 2007; Maja and Ehsani, 2010). The solution in many cases has been to use load cells to weigh the collected crop.

Durrence et al. (1999) developed a load cell-based yield monitor for peanut harvesters. Capacity load cells were fitted to the bin supports, and cumulative weights were recorded. Pelletier and Upadhyaya (1999) designed a load cell-based yield monitor for tomato crops. These authors decided to use a belt weigher for making load measurements, locating load cells in the last section of the boom elevator (just before the fruit is delivered to the truck). Miller and Whitney (1999) and Whitney et al. (2001) calculated the yield of citrus fruits using three different systems: a pressure transducer in the pressure line of a truck bed lifting system, four load cells under a truck bed, and a single load cell in a loader boom. Maja and Ehsani (2010) developed a yield monitoring system for citrus fruit mechanical harvesting involving a load cell-based impact plate. The system was modelled using either combinations of loads, springs and dampers, or using the energy balance equation. During field testing, the plate was installed at the end of the harvesting machine's fruit conveyor belt.

The Pellenc S.A. company (Pellenc and Bourely, 2001) developed a dynamic weighing system for grape harvesters in which grape clusters are weighed by two sets of load cells before they reach the collection bin. Arnó et al. (2005) tested another grape-weighing system involving a yield monitor and load cells located on the lateral discharge conveyor belt. Baguena (2011a) developed an on-board dynamic weighing system for grape harvesters, with load cells located directly under the bin. The main advantage of this is that the proper working of the system can be quickly verified. In this system, weight measurement is cumulative rather than instantaneous.

It is extremely important that the possible sources of error in yield monitoring systems be understood and taken into account. Blackmore and Marshall (1996) and Blackmore and Moore (1999) reported the effect on yield maps of errors associated with the topography of the terrain, volumetric calibration, unknown crop width on entry to the header, harvester fill mode, incorrect lag time, digital GPS (Global Positioning System) accuracy, and yield sensor accuracy. They concluded that the quality of data collected can be improved through the use of appropriate filters.

Although load cells may be certified for use in dynamic weighing systems, they are not error-free. The correction of the problems giving rise to these errors is an important area of sensor research. Makabe and Kohashi (2007) reported load cell errors such as hysteresis and creep owed to the design of the active part of the sensor. Hysteresis can be the consequence of the design a load cell and the properties of the materials used to make it. Improvements might therefore be obtained by constructing load cells with more appropriate materials. Hysteresis compensation methods have also been proposed (Makabe and Kohashi, 2004; Zijian and Renwen, 2002).

The topography of the terrain (the slope of fields) over which a harvester must move can cause errors in load cell measurements. In the laboratory, Fulton et al. (2009) subjected a combine harvester equipped with a yield monitor and a mass flow sensor (i.e., with no load cell) to different inclinations. Both transversal and especially longitudinal inclinations (0–8.5°) influenced the results returned by the weighing system. This same conclusion was reached by Baguena et al. (2011b), who examined the effect of inclination on an on-board dynamic weighing system that *did* involve load-cell measurements. The error was small when the machine was tested in the horizontal position – the natural orientation for its calibration – but became large at the most extreme inclinations. Both sets of authors suggested a compensation formula for minimising the effects of inclination.

Recently the discrete element method (DEM, Cundal and Strack, 1979) has been shown to predict the behaviour of moving granular material very well (Van Zeebroeck et al., 2006; Van Liedekerke et al., 2009; Ramírez et al., 2010a, 2010b; González-Montellano et al., 2011, 2012; Balevičius et al., 2011; Kobyłka and Molenda, 2013). In the present work, the DEM was used to simulate the displacement of the load inside a grape harvester bin in relation to its inclination. Different DEM models were developed, inclining the grape harvester forward and backward several times to reproduce changing terrain conditions. The redistribution of the load in the bin was shown to affect the results that would be provided by load cells under the bin. Recommendations to improve the accuracy of load cell measurements made in the field are proposed.

2. Materials and methods

2.1. Models

The DEM models constructed simulated the behaviour of the material in the bin of a classic grape harvester. Fig. 1 shows the shape of the bin, the walls of which are made of steel sheeting. Given the recommendations provided in the literature, the use of a load cell is assumed, located on a beam under the bin. The load cell estimates the mass of the material stored in the bin. The front of the bin is assumed to contain a hydraulic cylinder (Fig. 1a) to incline – and thus empty – the bin on demand.

Hydrogel spheres were used to represent grapes. This facilitated validation tests of the models – hydrogel spheres are neither perishable nor subject to seasonal availability. The mechanical properties of grapes and hydrogel spheres were assumed to be very similar.

All simulations were performed using EDEM Academic v2.3 (2010) software. In all cases, the interactions between particles and between particles and walls were represented by the Hertz–Mindlin contact model (Mindlin, 1949; Tsuji et al., 1992; Džiugys and Peters, 2001; Balevicius et al., 2006). Although grapes are not simple elastic bodies, this elastic, non-linear contact model is considered to be a good enough approximation for the purposes of this work. With the aim of taking into account energy dissipation in the system, viscous damping was contemplated in the normal and tangential directions for each contact, plus frictional damping in the tangential direction. The time step (Δ_t) in all simulations was constant at 1.47×10^{-4} s, i.e., at 20% of the critical time pass (Δ_{tc}) given by the Rayleigh time (t_R) (Li et al., 2005).

Values for the mechanical properties of the hydrogel spheres (Table 1) were determined experimentally when possible. Standardised, validated procedures were followed whenever available. When not, procedures proposed in the literature were used if possible; when no reliable procedure was available, values were fixed in agreement with the experience of the authors and modified if needed in accordance with the model validation process (Section 3.1).

In all models, the hydrogel spheres were represented as spherical particles of non-uniform size in agreement with the results of preliminary analyses of the real spheres. A normal size distribution was assumed, based on a mean diameter of $d = 8.85$ mm ($\sigma = 1.30$ mm). In order to simulate a more real situation, and to avoid instabilities in simulations owed to the presence of oversized or undersized particles (González-Montellano et al., 2011), the normal size distribution used was limited to $d_{min} = 0.85d$, and $d_{max} = 1.15d$.

2.2. Models constructed and simulation procedure

The simulation procedure followed for all DEM models involved two stages: a filling or static stage, and a dynamic stage. The filling stage was short, starting with the creation of the particles at some point inside the bin (which remained still throughout this stage) and ending with the pile of particles resting over the bottom of the bin. The generation of the particles was initiated at a virtual rectangular surface (Fig. 1b) located in the upper part of the bin. In fact, two such virtual surfaces were contemplated: VS1, which was smaller and located close to the front of the bin, and VS2, which was larger and covered the entire free surface of the bin. Both surfaces were deemed to be at a height $Z = 0.9$ m according to the reference system provided in Fig. 1. The particles were generated from these virtual surfaces in two ways: (1) by constant generation, in which particles are created continuously at a fixed generation rate (GR) until the final mass (W) of the particles is reached and (2) by discrete generation, in which W is fractionated into several parts with each part being created at regular times at a fixed generation rate (GR). The use of VS1 is aimed at establishing an initial particle distribution concentrated towards the front of the bin. In contrast, VS2 is used for generating an initially uniform distribution of particles. The use of one or the other virtual surface

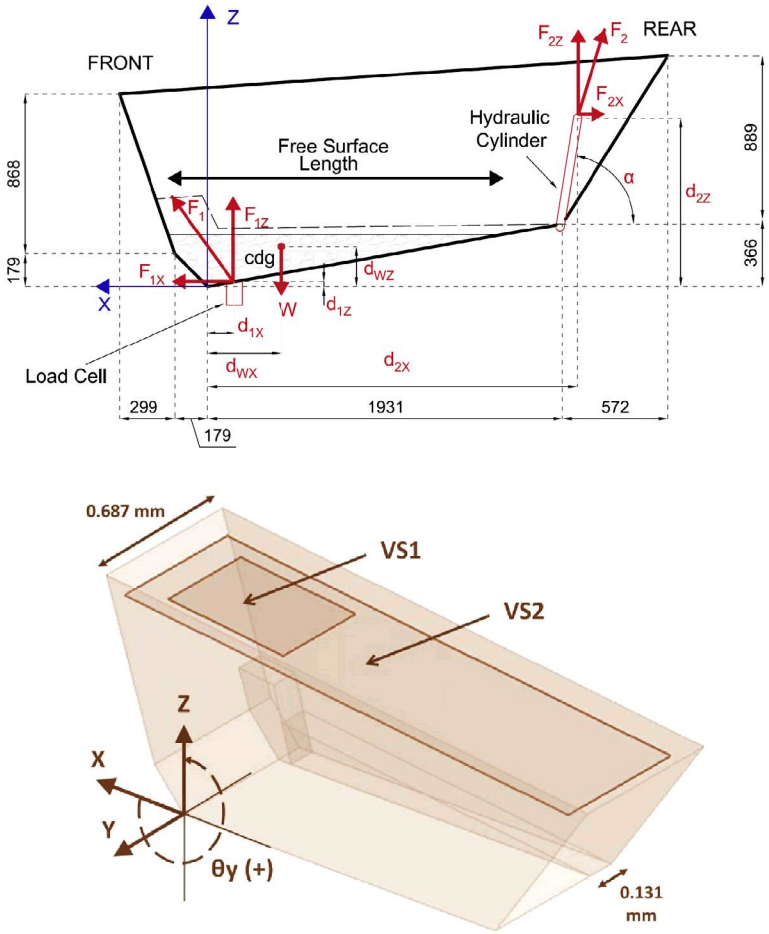

Fig. 1. Geometric characteristics of the grape harvester bin. (a) Two-dimensional view in the horizontal position ($\theta_y = 0°$) and (b) three-dimensional view.

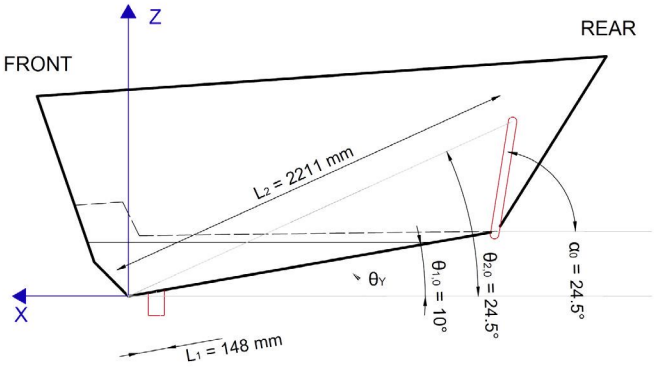

Fig. 2. Characteristic lengths and angles of the bin when in position $\theta_Y = 0°$.

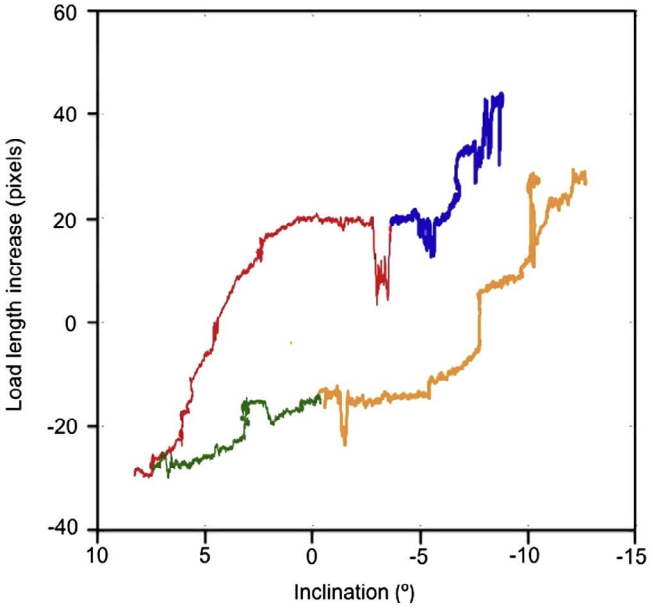

Fig. 3. Change in the experimentally-obtained FSL value.

allows the influence of the initial load distribution on the measurements returned by the load cell to be investigated.

The type of virtual surface, the particle generation system, and *W*, were different for the different DEM models (see Table 2).

The dynamic stage, which begins immediately after the static stage, sees the bin subjected to a sequence of forward and backward swings on its *Y* axis, according to the reference system in Fig. 1b. The sequence chosen was different for different the DEM models. However, in all cases the angle through which the bin moved (θ_y) was between a minimum of $\theta_{y,min} = -10°$ and a maximum of $\theta_{y,max} = 10°$. All the swing sequences contemplated involved six consecutive phases, each assuming a bin movement from an initial position of $\theta_y = 0°$ to a final position of $\theta_{y,max}$ or $\theta_{y,min}$ or *vice versa*. The inclination rate (ω_y) was held constant during each phase of the swing sequence. However, these sequences could include intercalated halts, at which $\omega_y = 0$. Figs. 4–8 show the

Table 1
Mechanical properties contemplated in the construction of the DEM models.

Property		Value	Determination methodology
Density (kg/m^3)	ρ_p	1035	Pycnometer test (ASTM D854–10, 2010)
Stiffness (Pa)	E_p	10^6	Parallel plate compression test (ASAE S368.4 (2006))
Poisson's ratio	ν_p	0.24	Estimated from author experience
Particle-wall restitution coefficient	e_w	0.8	Drop test (González-Montellano et al., 2012)
Particle-r coefficient	e_p	0.7	Estimated from author experience
Particle-wall friction coefficient	μ_w	0.05	Estimated from author experience
Particle-particle friction coefficient	μ_p	0.05	Estimated from author experience

Table 2
Characteristics of the constructed models.

Load (kg)	Model number	Virtual surface	Particle generation type	W (kg)	Itinerary
75	M1	VS1	Constant (GR = 40 kg/s)	75	S1
	M2	VS1	Constant (GR = 40 kg/s)	75	S2
	M3	VS1	Constant (GR = 40 kg/s)	75	S3
450	M4	VS1	Discrete: 50 kg ever 2 s (GR = 40 kg/s)	450	S4
750	M5	VS2	Discrete: 50 kg every 2 s (GR = 40 kg/s)	750	S5

S1: $\omega_y = 2°/s$, with a 4 s halt once maximum inclination reached; S2: $\omega_y = 2°/s$, no halt; S3: $\omega_y = 4°/s$, with no halt; S4, as for S2; S5 as for S2. GR: generation rate.

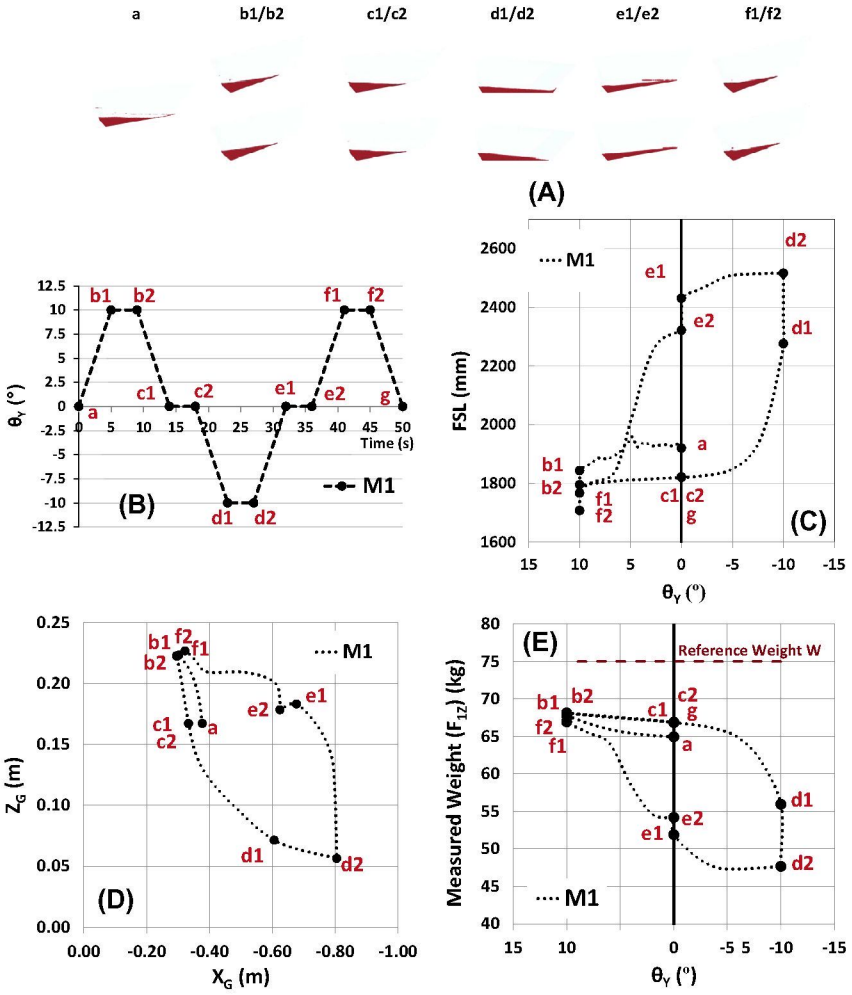

Fig. 4. Results obtained for M1: (A) position of the harvester and distribution of the load at different times; (B) swing sequence; (C) change in bin free surface length (FSL); (D) change in the centre of gravity; and (E) change in the vertical load recorded by the load cell.

characteristics of the sequences (stages, ω_y, and intercalated halts) contemplated in each DEM model. Different sequence types were thus chosen: (1) S1, in which $\omega_y = 2°/s$, with a 4 s halt once the maximum inclination was reached; (2) S2, in which $\omega_y = 2°/s$, with no halt; (3) S3, in which $\omega_y = 4°/s$, with no halt; (4) S4, the same as S2 but under heavy load conditions; and (5) S5, also the same as S2

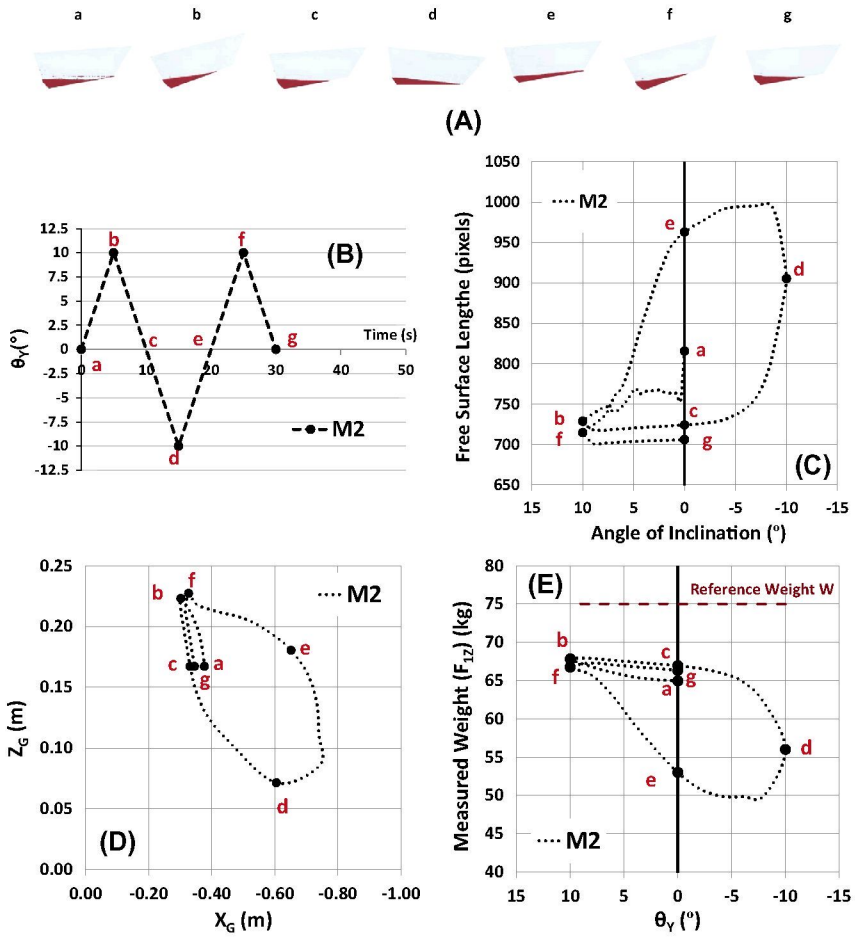

Fig. 5. Results obtained for M2: (A) position of the harvester and distribution of the load at different times; (B) swing sequence; (C) change in bin free surface length (FSL); (D) change in the centre of gravity; and (E) change in the vertical load recorded by the load cell.

buy under very heavy load conditions. Modifying the movement of the bin in this way allows the passage of the harvester over areas of ascending or descending slope to be simulated. The use of different ω_y values allows the influence of the inclination rate to be investigated. Those times at which $\omega_y = 0°/s$ are representative of areas of constant slope.

Through the combination of the possibilities described above, five DEM models were constructed to study the influence of the displacement of the load, which would influence the mass recorded by the load cell. To reduce the computational effort required, three initial DEM models involving small loads (M1, M2 and M3) were constructed to study the effect of the inclination rate ω_y. Then, with the aim of studying a more lifelike situation, two further DEM models were constructed – M4 and M5 – to examine the influence of larger loads and their initial distribution in the bin. Table 2 summarises the characteristics of each of these models.

2.3. Variables taken into account in the analysis of the numerical results

Since the displacement of the load would affect the readings returned by the load cell, three variables were taken into account in the analysis of the numerical results provided by the models: the variation in the bin free surface length (FSL, defined as the length of the bin (on its *X* axis) occupied by the material carried at any given time and bin position), the change in the centre of gravity (CoG) of this material, and the variation in the load detected by the load cell.

2.3.1. Change in the load free surface length

The FSL (Fig. 1a) reflects the concentration of particles at the extreme anterior part of the bin, i.e., in the proximity of the load cell. Changes in the FSL are easily observed in real, working harvesters. Thus, the FSL not only serves as a variable for analysing the DEM models, it can also be used in validation tests (see Section 2.4). Using MATLAB software, colour analysis computation techniques were used to calculate the FSL from the numerical results and in later validation tests. These techniques were employed to analyse different images of the bin (both in the DEM models and validation tests) taken in the negative direction of the *Z* axis, at different times during the swing sequence.

2.3.2. Change in the centre of gravity

The CoG summarises the distribution of the particles in the bin at any given moment, and is vital for estimating the load detected by the load cell at any time in a swing sequence. At such a moment, the coordinates of the CoG (X_G, Y_G, Z_G) can be determined thus:

$$X_G = \frac{\sum_i X_i \cdot m_i}{\sum_i m_i}; \tag{1}$$

$$Y_G = \frac{\sum_i Y_i \cdot m_i}{\sum_i m_i}; \tag{2}$$

$$Z_G = \frac{\sum_i Z_i \cdot m_i}{\sum_i m_i} \tag{3}$$

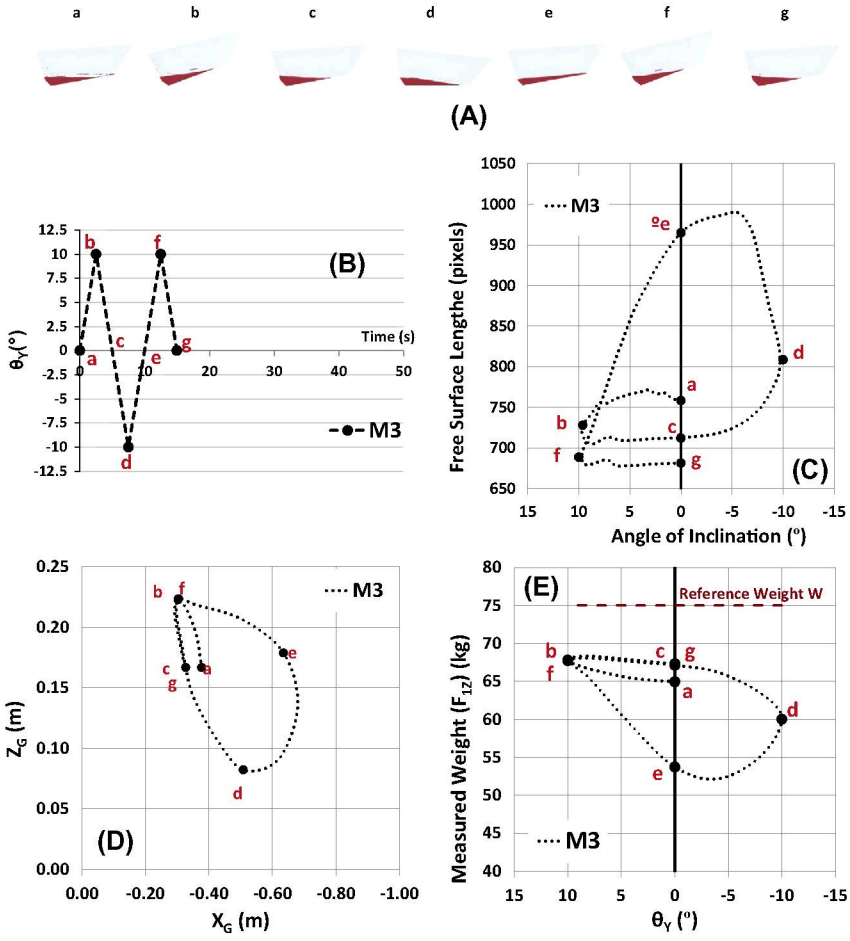

Fig. 6. Results obtained for M3: (A) position of the harvester and distribution of the load at different times; (B) swing sequence; (C) change in bin free surface length (FSL); (D) change in the centre of gravity; and (E) change in the vertical load recorded by the load cell.

where X_i, Y_i, Z_i are, respectively, the coordinates X, Y and Z (according to the reference system given in Fig. 1) of each of the particles 'i' in the bin, and where m_i is the mass of each of the particles i contemplated.

Three-dimensional DEM models studied in this work showed a relatively constant value of Y_G and close to the value of half the width of the bin (YG ≈ 681/2 ≈ 340 mm). This is explained by the fact that all the swings were executed about the Y axis, which makes the load in the bin remain evenly distributed along that axis. For this reason, results and conclusions shown in Section 3 will only focus on observations made within the XZ plane. It should be noted that in a real working situation, ground conditions may be much more complex than those contemplated in this work. In this case, load displacements along the Y axis would be of importance. However, these effects will be studied in future works.

2.3.3. Change in F_{1z}: an estimation of the vertical load detected by the load cell

The vertical load that would be detected by the load cell or a real harvester will be estimated from the numerical results provided by the DEM models via simple force balancing. The stored mass W (Table 2) is considered to act at the CoG, and must be counteracted by two forces, F_1 and F_2, respectively developed at the point of union between the bin and the load cell and the bin and the hydraulic cylinder. Both forces can be decomposed into directions X and Y (Fig. 1a), resulting in the system of forces shown in Fig. 1a. The resolution of this system of forces provides the value of the components F_{1x}, F_{1z}, F_{2x} and F_{2z}, with the value of F_{1z} affording an estimate of the vertical load that would be detected by the load cell of a real grape harvester. This resolution process involves the use of equations representing the force balance (in the X and Z directions) and the moment balance (about Y axis). These equations are expressed thus:

$$F_{1x} - F_{2x} = 0 \tag{4}$$

$$F_{1z} - F_{2z} = P \tag{5}$$

$$F_{1x}d + F_{1z}d - F_{2x}d_{2z} + F_{2z}d_{2x} = Wd_{WX} \tag{6}$$

where d_{1x}, d_{1z}, d_{2x}, d_{2z} are the horizontal and vertical distances from the point of action of F_1 and F_2, measured with respect to the bin's lowest point. These values can be perfectly well known since the geometry of the bin is known. The value of d_{WX} is the value of the horizontal coordinate (X_G) of the CoG of the mass, the point where the force of W acts. The value of d_{WX} is variable, depending on the distribution of the particles in the bin during the swing sequence followed in each DEM. Thus, the value of F_{1z} – the mass detected by the load cell – will vary over the swing sequence.

Eqs. (4) and (6) represent a system of three equations with four unknowns (F_{1x}, F_{1z}, F_{2x} and F_{2z}). An additional condition must therefore be set if the system is to be resolved. This condition comes from Eq. (7), which expresses the relationship between F_{2x} and F_{2z}, imposed by the magnitude of the angle α formed between the hydraulic cylinder and the horizontal at any given instant.

$$tg(\alpha) = F_{2z}/F_{2x} \tag{7}$$

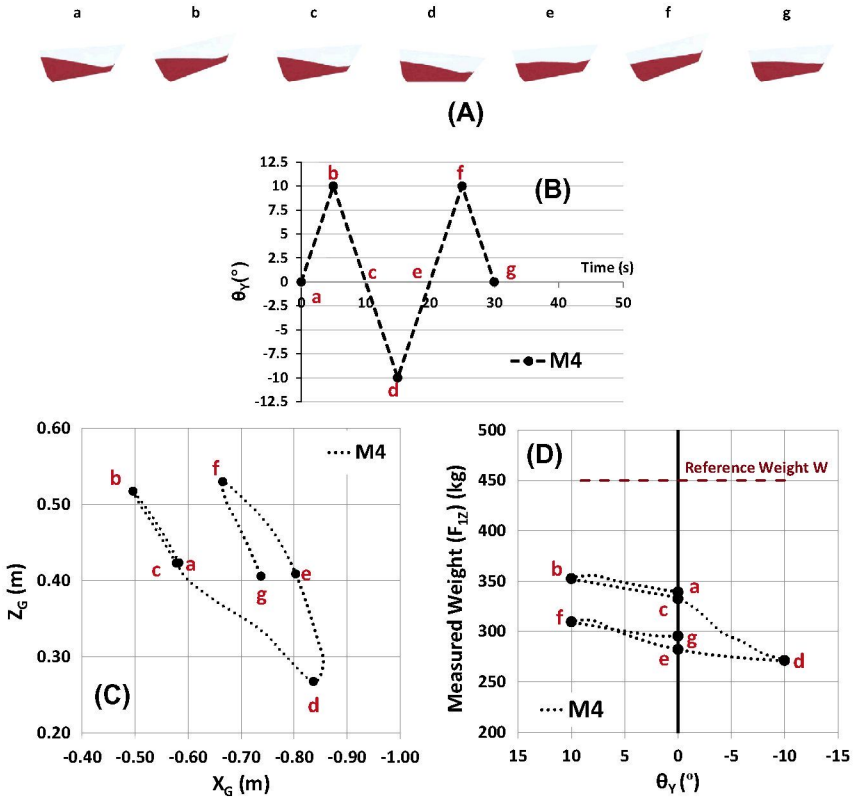

Fig. 7. Results obtained for M4: (A) position of the harvester and distribution of the load at different times; (B) swing sequence; (C) change in bin free surface length (FSL); (D) change in the centre of gravity; and (E) change in the vertical load recorded by the load cell.

The values of d_{1x}, d_{1z}, d_{2x}, d_{2z} and α also vary depending on the angle of inclination θ_Y of the bin at any moment. The determination of these values with respect to θ_Y is determined as shown below:

$$d_{1x} = L_1 \cdot \cos(\theta_{1,0} + \theta_Y) \tag{8}$$

$$d_{1z} = L_1 \cdot \text{sen}(\theta_{1,0} + \theta_Y) \tag{9}$$

$$d_{2x} = L_2 \cdot \cos(\theta_{2,0} + \theta_Y) \tag{10}$$

$$d_{2z} = L_2 \cdot \text{sen}(\theta_{2,0} + \theta_Y) \tag{11}$$

$$\alpha = \alpha_0 + \theta_Y \tag{12}$$

where L_1, L_2, $\theta_{1,0}$, $\theta_{2,0}$ and α_0 are characteristic lengths and angles when the bin is in the position $\theta_Y = 0°$ (Fig. 2).

Once d_{1x}, d_{1z}, d_{2x}, d_{2z} and α are known for each instant in the swing sequence in each DEM model, the above four-equation system (Eqs. (4)–(7)) can be used to determine F_{1x}, F_{1z}, F_{2x} and F_{2z}, with F_{1z} being the load detected by the load cell at any given instant. The value of F_{1z} will appear to closer to the true value of W when the CoG is over the vertical that passes through the load cell (when $d_{1x} \approx d_{wx}$).

2.4. Experimental validation of the DEM models

To guarantee the representativeness of the constructed DEM models, the contact model (Hertz–Mindlin) used was carefully chosen, and most of the properties of the hydrogel spheres determined experimentally. However, only validation testing can ensure such representativeness. An experiment was thus performed with a real bin in which the conditions simulated by M2 (although any other model could have been chosen) applied. The numerically- and experimentally-obtained FSL values (see Section 3.1) were then compared.

3. Results and discussion

3.1. Model validation and introductory remarks

3.1.1. Model validation

Fig. 3 shows the change in the FSL value obtained with the real bin in the above validation test (Baguena et al., 2011b); the results are very similar to those shown in Fig. 5b, which shows the numerically-obtained results for FSL in M2. This guarantee of representativeness can be extended to the other DEM models constructed.

3.1.2. Introductory remarks

The results for the different DEM models are shown in separate figures and diagrams that provide: (1) illustrations of the starting and end points of each stage in the swing sequence; (2) the characteristics of the swing sequence followed, including the angle of inclination θ_Y of the bin with respect to time (with time zero being the start of the dynamic stage); (3) the change in FSL over the swing sequence; (4) the change in the CoG of the mass inside the bin during the sequence swing; and (5) the change in the vertical load F_{1z} – an estimation of the load that would be detected by the load cell – (over the swing sequence. Figs. 4–6 show these data for M1, M2 and M3; Figs. 7 and 8 show the same for M4 and M5 with the exception of the FSL values (the larger quantity of particles in the bin rendered the FSL result non-representative of the arrangement of the load; the load covers the entire bin floor).

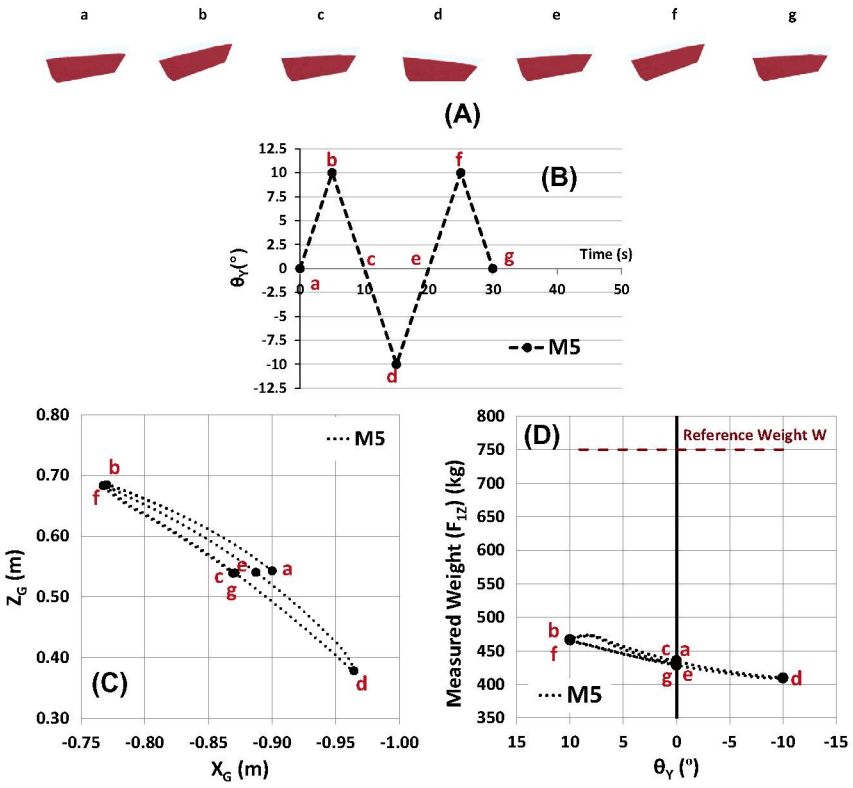

Fig. 8. Results obtained for M5: (A) position of the harvester and distribution of the load at different times; (B) swing sequence; (C) change in bin free surface length (FSL); (D) change in the centre of gravity; and (E) change in the vertical load recorded by the load cell.

3.2. Results for M1, M2 and M3

3.2.1. M1

M1 (Fig. 4) represents a situation in which the harvester covers a terrain with slight changes in its slope ($\omega_y = 2°/s$), intercalated with areas of constant slope ($\omega_y = 0$). Although the particles were generated by VS1, the small load meant the particles assumed an initial uniform distribution (point 'a' in the swing sequence).

3.2.1.1. Change in the load free surface length. When the bin tips forward (stage a–b1), the material concentrates slightly in the anterior region. This leads to a slight reduction in the FSL (Fig. 4C). The bin is then halted (stage b1–b2) at an inclination angle of $\theta_Y = 10°$, although the FSL continues to fall with the material concentrated in the same area – the result of the inertia it acquired in the previous stage. The bin then begins to incline backwards (stage b2–c1), but the FSL hardly changes since the particles are still subject to inertia, now acting in the opposite direction. Finally, the bin recovers its initial angle of inclination ($\theta_Y = 0°$) and remains at this through the next stage (stage c1–c2), with the FSL remaining constant.

.The bin is then tipped backward again but at a steeper angle (stage c2–d1), and the material is strongly displaced, and ends up covering the entire bin floor. This is associated with a notable increase in FSL. The bin is then halted (stage d1–d2), but the FSL continues to rise due to the inertia acquired by the particles.

By the time the latter period is over, the particles have lost much of their inertia. Thus, when the bin is newly tipped forward (stage d2–e1), the FSL falls, although not by very much. By the end of this tipping, the particles have again acquired some inertia, such that when the next halt begins (stage e1–e2), the FSL continues to fall.

This is followed by a new swing forward (stage e2–f1) during which a notable reduction in the FSL is seen, caused by the particles still conserving a certain forward inertia. The FSL value reached is lower even than at the beginning of the sequence. The fall continues somewhat during the next halt (stage f1–f2).

Finally, the bin is tipped forward again (stage f2–g), with the FSL reaching a value coincident with that seen at points c1 and c2. If the sequence were to continue, the FSL would go through the same cycle of values described between points c1 and g.

These results show that the inertia acquired by the particles plays an important role in the way they arrange themselves in the bin. When the bin begins to swing again (in the opposite direction) after a halt (e.g., in stages b2–c1, d2–e1 and f2–g), the FSL is only slightly modified. Under these conditions the particles hardly show any inertia. However, when the bin continues to swing in the same direction after a halt (stages c2–d1 and e2–f1) the particles show greater inertia, and the FSL changes more quickly.

3.2.1.2. Change in the centre of gravity. The displacements experienced by the load during the swing sequence cause the CoG of the mass in the bin to change (Fig. 4D) on both the *Z* and *X* axes. This change is analogous to the changes seen in FSL. Thus, increases in FSL (stages b2–c1, c2–d1 and d1–d2) provoke a reduction in the absolute value of Z_G and an increase in the absolute value of X_G. The opposite occurs when FSL decreases (stages d2–e1, e1–e2 and e2–f1).

3.2.1.3. Change in the vertical load F_{1z}. The vertical load that would be detected by the load cell of the simulated bin can be approximated from the value of F_{1z}, which is calculated as described in stage Section 2.3.3. The value of F_{1z} for a given bin position and load *W* is strongly dependent on the value of X_G. When $X_G = 0$, F_{1z} is equal to the value of *W*. In this scenario, the load cell will

register W in its entirety since the CoG coincides with the vertical passing through the load cell. However, as the absolute value of X_G increases, the greater the difference between F_{1z} and W becomes since some of the mass in the bin is taken by the hydraulic cylinder.

Given the above, the change in F_{1z} over the swing sequence is analogous to that described for the CoG. Fig. 4E shows how, at any position during the swing sequence, F_{1z} is always less than the true value of W. This occurs because the absolute value of X_G is always greater than zero, causing the hydraulic cylinder to assume support for part of the load. In fact, the greater the values of X_G, the smaller that of F_{1z}, and, therefore, of the error in the result returned by the load cell. In the best case scenario, i.e., when the bin is fully tipped forward (points b1–b2 and f1–f2) and the bin's contents are concentrated close to the load cell, the actual load detected would be 0.9 W. In the worst case scenario, i.e., when the bin's contents are extended across the bin floor (points d1 and d2), the load detected would be 0.6 W.

3.2.2. M2

M2 (Fig. 5) represents a situation in which the harvester does not experience extreme variations in the slope of the terrain ($\omega_y = 2°/s$) nor are there any halts. As in M1, the initial arrangement of the particles (point 'a' in the swing sequence) is uniform.

3.2.2.1. Change in the bin free surface length. The changes in FSL are similar to those seen in M1. However, in M2, the absence of halts following a swing generates inertia in the particles that acts in the opposite direction of any new swing. Thus, the maximum values of FSL are smaller than those seen in M1, and the particles therefore less spread out over the bin floor.

When the bin begins a new swing (e.g., forwards, as in stage a–b), the particles begin to move in this direction and acquire more and more inertia. When the swing is complete, no halt follows. Rather, the bin begins to swing in the opposite direction. In the first instants of this new swing, the particles show an initial inertia in the opposing direction, reducing their displacement in the new swing direction. Thus, the FSL remains practically unchanged over stage b–c, even though an increase in its value may have been expected.

The above effect is even stronger when the bin swings in the first direction for longer. For example, over stage b–d, the bin swings constantly forward, and the particles gather more and more inertia in this direction. In fact, the FSL increases strongly during the second half of this swing period (stage c–d). When the swing is complete (point d), the bin begins to swing back again (stage d–e), and a reduction in FSL might be expected. However, the large inertia acquired by the particles causes the FSL to continue increasing over the first part of the new swing. Indeed, the FSL does not begin to drop for some time, i.e., not until reaching the moment at which the opposing inertia is fully counteracted by the inertial forces imposed by the new swing. Consequently, FSL only falls slightly over stage d–e, generating a lower maximum FSL than in M1.

3.2.2.2. Change in centre of gravity. As with M1, the CoG changes in accordance with the FSL. Once again, an increase in FSL is associated with a reduction in Z_G and an increase in the absolute value of X_G, while a reduction in FSL leads to the opposite. However, in the present model, the less complete extension of the particles across the bin floor causes the absolute value of X_G to be always lower than that seen in M1.

3.2.2.3. Change in the vertical load F_{1z}. As with M1, the change in the vertical load F_{1z} depends directly on the change in the CoG of the bin's contents. In this model, the displacement of the CoG with respect to the vertical passing through the load cell is less than that seen in M1. Thus, the load detected by the cell is generally closer to the true value of W. In fact, the load detected (F_{1z}) varies between 0.67 W and 0.9 W, a smaller range than seen in M1.

3.2.3. M3

M3 (Fig. 5) represents a working situation for the harvester similar to that in M2. However, in this model, the inclination rate is greater ($\omega_y = 4°/s$). As in M1 and M2, the initial arrangement of the particles (point a) is uniform.

3.2.3.1. Change in the bin free surface length. In M3, the change in FSL is very similar to that observed in M2. However, the greater inclination rate of M3 means the inertia acquired by the particles is greater than in M2. The inertia opposing any swing in the opposite direction is therefore greater, causing an even greater reduction in FSL values than seen in M1 or M2.

3.2.3.2. Change in the centre of gravity. The change in CoG follows the qualitative trend seen in M2. However, as the change in FSL shows, the displacement of the load is less. Consequently, the modification of the CoG in M3 is notably less than in M1 or M2.

3.2.3.3. Change in the vertical load F_{1z}. The smaller changes in the CoG generate a smaller variation in F_{1z} obtained from the simulations the range of variation covered is 0.7–0.9 W. The maximum load detected is therefore similar in M1, M2 and M3; the main difference between the models is the minimum load detected.

3.3. High load models: M4 and M5

3.3.1. M4

M4 (Fig. 7) represents a working scenario for the harvester very similar to that described in M2, with only small changes in slope and no halts between swings. However, the load is much greater (450 kg compared to 75 kg), and its initial distribution is not uniform but concentrated near the load cell. This allows the effect of the initial distribution of the load on the value returned by the load cell to be examined.

3.3.1.1. Change in the centre of gravity. Although the load is initially concentrated near the load cell, the initial value of X_G (at point a) is, in absolute terms, greater than in M1–M3. This is a consequence of the higher load considered in this model, which displaces the CoG towards the central part of the bin. The change in the CoG follows the same rules as in the earlier models: X_G falls when the bin tips forward, and increases when it moves in the opposite direction. However, the way in which the load becomes redistributed over the swing sequence greatly affects X_G. Over the first two swings (stages a–b and b–c), the absolute value of X_G experiences a respective reduction and increase. Over these first two swings, the non-uniform distribution of the load is maintained, almost without change. However, in stage c–d it becomes much more uniform and the absolute value of X_G becomes much greater than in the last stage (b–c). From this moment on, the load is uniform, and remains so. The increase or reduction in the absolute value of X_G with each new swing therefore remains the same. Thus, in stages d–e and e–f, in which the bin tips forward, the reductions in the absolute value of X_G are very similar. Later, in stage f–g, the bin tips backwards, and the absolute value of X_G increases by the value it was reduced in the two previous stages. Thus, the value of X_G at the final point g does not coincide with its value at a, even though these points in the swing sequence are analogous. This is all due to the distribution of the load becoming uniform over stage c–d – a modification that notably attenuates the effect of the inertia seen in M1–M3. Repeating the swing sequence would give rise to a cyclical behaviour (arround points d–e–f–g–d) for the value of X_G.

3.3.1.2. Change in the vertical load F_{1z}. As in all the previous models, the change in the vertical load (F_{1z}) is completely dependent on the change in X_G, its absolute value inversely proportional to the load detected. The best approximation to W is achieved at point b (0.77 W), the worst at point d (0.61 W). However, if the cyclical behaviour for the value of X_G is taken into account (a behaviour that would occur after the load becomes uniform), the range of values detected would be 0.61–0.71 W. This is quite a small range, and quite different to those observed for the small load models M1–M3. This is a consequence of the greater load in the bin, which attenuates the effects of particle inertia as it becomes more uniformly distributed.

3.3.2. M5

M5 (Fig. 8) describes a work situation for the harvester identical to that in M4, except that the initial load is now 750 kg and uniformly distributed from the beginning of the swing sequence.

3.3.2.1. Change in the centre of gravity. The presence of the large load and its uniform arrangement means M5 is similar to M4 once the load becomes uniform in the latter model. The increases and reductions in X_G seen when the bin tips backward and forward respectively, are practically the same in absolute terms (although with opposite signs) for swings of the same duration. The values recorded are lower than in the other models. These effects are the consequence of the size of the load and its constantly uniform distribution.

3.3.2.2. Change in the vertical load F_{1z}. The change in the vertical load F_{1z} is analogous to the change in the coordinate X_G. When the absolute value of X_G is low (e.g., at points b or f, when the bin is completely tipped forward), a maximum load of 0.63 W is detected. A minimum load value of 0.56 W is returned when the absolute value of X_G is higher (point d, at which the bin is fully tipped backward). Thus, in this model, the load cell underestimates W much more than in M1–M4, although the range of variation of the results returned is much smaller.

3.4. Accurate estimation of the mass of material carried in the bin

The present results show that the load detected by the load cell is always less than the true mass of the bin's contents. This is due to the displacement of the CoG with respect to the vertical passing through the load cell, such that part of the total load W becomes supported by the hydraulic cylinder, reducing that detected by the load cell.

A possible solution lies in the mathematical correction of the value recorded. This would involve knowing the mathematical relationships between the error in recording and the many variables that affect it (the movements in a swing sequence, initial distribution of the load, the true starting mass etc.) However, this would be very complex, made even more complicated by the changing nature of these variables as the harvester continues its work. An efficient way of calculating the real load W inside the bin would be to measure the force developed on the hydraulic cylinder (F_2, Fig. 1a) as well as that detected by the load cell (F_{1z}). If both these values are known, along with the angle of inclination of the cylinder (α) at each instant, a modified form of Eq. (5) could be used (Eq. (13)) to determine W:

$$W = F_{1z} + F_2 \mathrm{sen}(\alpha) \tag{13}$$

The success obtained would depend on the accuracy of the measurement of the variables involved. One of the values with most uncertainty is that of the force developed by the hydraulic cylinder. To determine the admissible margin of error in the determination

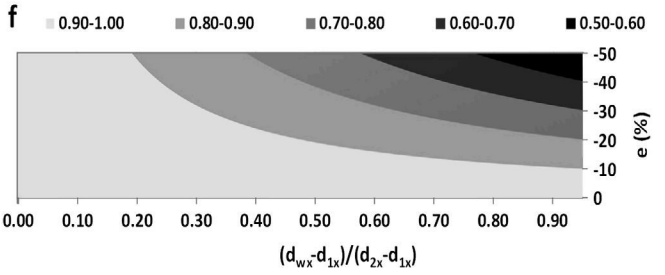

Fig. 9. Value of f for different positions of the centre of gravity of the load and for different errors e (%) made in the measurement of F_2.

of F_2, consider a factor 'f' that represents that represents the ratio of the weight detected using Eq. (13) (considering that F_2 has been obtained with an error 'e' (%)) to the true value of the weight W. Consider then a bin with a content of mass W, with a CoG at a horizontal distance d_{wx} from the lowest point of the bin (see Fig. 1a). In this scenario, F_{1z} is the vertical force detected by the load cell, and F_2 the force on the hydraulic cylinder (with annclination α) required to reach equilibrium. Suppose that at this point the value of the force developed in the cylinder is measured with an error e (%), i.e., a measured force on the cylinder of $(1 + e/100)F_2$. The fraction f of the total W measured under such circumstances is then given by Eq. (14):

$$f = \frac{F_{1z} + (1 + e/100)F_2 \mathrm{sen}(\alpha)}{W} \tag{14}$$

Fig. 9 shows the values of f obtained for different load distributions and errors e; W was set at 450 kg, although this would not affect f since proportionality exists between F_{1z}/F_2 and W. The horizontal axis shows the magnitude of the horizontal distance between the load cell position and the CoG of the mass. This distance is expressed via the a dimensional variable $\zeta_w = (d_{wx} - d_{1x})/(d_{2x} - d_{1x})$. Finally, in the vertical axis the error e (%) in the measurement of F_2 is shown. The different shades in the figure identify the values of f obtained for each combination of e and ζ_w.

Fig. 9 shows that any negative error in the measurement of F_2 ($e < 0$) generates a value for f of 0.5–1, thus implying an underestimation of the mass of the bin's contents. However, large absolute values for e do not necessarily mean low f values. In fact, e values of up to 50% are compatible with f values of >0.9 as long as the CoG is close to the load cell (low ζ_w values). In such situations, the fraction of W supported by the hydraulic cylinder would be relatively low, and therefore a high error e in its measurement would have no determining effect on the final value of W given by Eq. (13). Under the conditions studied in the present work (inclinations $-10° < \theta_Y < 10°$ and inclination rates of $-4°/s < \omega_Y < 4°/s$), ζ_w would always be $\leqslant 0.4$. Thus, in general, errors of up to 20% in the determination of F_2 should provoke no great error in the estimation of W ($f > 0.9$). Nonetheless, the more accurate the measurement of the force developed by the hydraulic cylinder, the more accurate the estimation of W.

4. Conclusions

In this work, the variations of the load registered by the load cell of a grape harvester have been investigated by means of the discrete element method. Although the use of this method is relatively new in such applications, it has provided essential data to obtain the results presented in this research, In addition, it has proven once more its capability for simulating the real behaviour of granular assemblies of different nature.

All the models constructed showed the true mass W of the bin's contents would be underestimated by a dynamic weighing system involving a load cell. The load recorded is highly affected by the distribution of the load inside the bin – which is not only influenced by the inclination of the bin at a given instant but by the history of its inclination (the change in the slope, and the presence of halts between swings, etc.). The effect of the inertia acquired by the particles making up the load is not negligible. Given the many variables that influence the accuracy of load cells, no systematic and instantaneous correction of their readings would seem possible. However, if the force developed in the hydraulic cylinder were recorded as well, mathematical corrections could be made, and the true mass of the harvested crop could be more accurately determined.

Acknowledgements

Some of the experimental data used for validation in this paper were generated in a joint research at the Katholieke Universiteit Leuven (Belgium) in collaboration with the CNH Belgium. The authors are grateful to the technical staff working in the Department of Biosystems at Katholieke Universiteit Leuven, as well as the technical staff from CNH Belgium, giving the necessary support and co-operation. The funding of this work has been covered by LPF-TAGRALIA research group together with the Universidad Politécnica de Madrid, and the Spanish Plan for Research, Development and Innovation through the research project AGL2012-39994-C03-02.

References

Arnó, J., Bordes, X., Ribes-Dasi, M., Blanco, R., Rosell, J.R., Esteve, J., 2005. Obtaining grape yield maps and analysis of within-field variability in Raimat (Spain). In: Proceedings 5th European Conference on Precision Agriculture, Uppsala, Sweden, June 8–11, pp. 899–906.

ASAE S368.4, 2006. Compression test of food materials of convex shape. American Society of Agricultural and Biological Engineers (ASABE).

ASTM D854–10, 2010. Standard test methods for specific gravity of soil solids by water pycnometer. American Society for Testing and Materials (ASTM).

Balevicius, R., Dziugys, A., Kacianauskas, R., Maknickas, A., Vislavicius, K., 2006. Investigation of performance of programming approaches and languages used for numerical simulation of granular material by the discrete element method. Computer Physics Communications 175 (6), 404–415.

Balevičius, R., Kačianauskas, R., Mróz, Z., Sielamowicz, I., 2011. Analysis and DEM simulation of granular material flow patterns in hopper models of different shapes. Advanced Powder Technology 22 (2), 226–235.

Baguena, E.M., 2011a. On-board system for yield and quality determination in grape harvesters: development and field validation. PhD Dissertation, Universidad Politécnica de Madrid.

Baguena, E.M., Barreiro, P., Valero C., Missotten, B., Verhoeven, J., De Baerdemaeker, J., Saeys, W., 2011b. Analysis of load displacement in grape harvesters and corresponding effect on dynamic weighing system under laboratory conditions. In: Proceedings 8th European Conference on Precision Agriculture, Prague, Czech Republic, July 11–14, pp 390–399.

Birrell, S.J., Sudduth, K.A., Borgelt, S.C., 1996. Comparison of sensors and techniques for crop yield mapping. Computers Electronics Agriculture 14, 215–233.

Blackmore, B.S., Marshall C.J., 1996. Yield mapping: errors and algorithms. In: Proceedings 3th International Conference on Precision Agriculture, Minneapolis, EEUU, June 23–26, pp. 403–416.

Blackmore, S., Moore, M., 1999. Remedial correction of yield map data. Precision Agriculture 1, 53–66.

Colvin, T.S., Karlen, D.L., Tischer, N., 1991. Yield variability within fields in central Iowa. In: Proceedings of the 1991 Symposium on Automated Agriculture for the 21st Century, Chicago, EEUU, December 16–17, pp. 366–372.

Cundal, P., Strack, O., 1979. A discrete numerical model for granular assemblies. Geotechnique 29 (2), 47–65.

Durrence, J.S., Hamrita, T.K., Vellidis, G., 1999. A load cell based yield monitor for peanut feasibility study. Precision Agriculture 1, 301–317.

Džiugys, A., Peters, B., 2001. An approach to simulate the motion of spherical and non-spherical fuel particles in combustion chambers. Granular Matter 3 (4), 231–266.

EDEM, 2010. EDEM 2.3 user guide. DEM Solutions Ltd., Edinburgh, Scotland (UK).

Fulton, J.P., Sobolik, C.J., Shearer, S.A., Higgins, S.F., Burks, T.F., 2009. Grain yield monitor flow sensor accuracy for simulated varying field slopes. Applied Engineering in Agriculture 25, 15–21.

González-Montellano, C., Ramírez, Á., Gallego, E., Ayuga, F., 2011. Validation and experimental calibration of 3D discrete element models for the simulation of the discharge flow in silos. Chemical Engineering Science 66 (21), 5116–5126.

González-Montellano, C., Fuentes, J., Ayuga-Téllez, E., Ayuga, F., 2012. Determination of the mechanical properties of maize grains and olives required for use in DEM simulations. Journal Food Engineering 111 (4), 553–562.

Kobyłka, R., Molenda, M., 2013. DEM modelling of silo load asymmetry due to eccentric filling and discharge. Powder Technology 233, 65–71.

Li, Y., Xu, Y., Thornton, C., 2005. A comparison of discrete element simulations and experiments for sandpiles composed of spherical particles. Powder Technology 160 (3), 219–228.

Magalhães, P.S.G., Cerri, D.G.P., 2007. Yield monitoring of sugar cane. Biosystems Engineering 96, 1–6.

Maja, J., Ehsani, R., 2010. Development of a yield monitoring system for citrus mechanical harvesting machines. Precision Agriculture 11, 475–487.

Makabe, M., Kohashi, T., 2004. Practical creep and hysteresis error compensation method for load cell. In: SICE Annual Conference, Sapporo, Japan, August 4–6, pp. 77–83.

Makabe, M., Kohashi, T., 2007. High accurate creep compensation method for load cell. In: 46th SICE Annual Conference, Takamatsu, Japan, September 17–20, pp. 29–36.

Miller, W.M., Whitney, J.D., 1999. Evaluation of weighing systems for citrus yield monitoring. Applied Engineering Agriculture 15, 609–614.

Mindlin, R., 1949. Compliance of elastic bodies in contact. Journal Applied Mechanics 71, 259–268.

Pellenc, R., Bourely, A., 2001. On-board device and method for continuous weighing of harvest and harvesting machines using same. Patent Number: US 06283853. Official Gazette of the United States Patent and Trademark Office Patents.

Pelletier, G., Upadhyaya, S.K., 1999. Development of a tomato load/yield monitor. Computers Electronics Agriculture 23, 103–117.

Ramírez, A., Nielsen, J., Ayuga, F., 2010a. On the use of plate-type normal pressure cells in silos: Part 1. Calibration Evaluation Computers Electronics Agriculture 71, 71–76.

Ramírez, A., Nielsen, J., Ayuga, F., 2010b. On the use of plate-type normal pressure cells in silos: Part 2. Validation for pressure measurements. Computers Electronics Agriculture 71, 64–70.

Stafford, J.V., Ambler, B., Smith, M.P., 1991. Sensing and mapping grain yield variations. In: Proceedings of the 1991 Symposium on Automated Agriculture for the 21st Century, Chicago, EEUU, December 16–17, pp. 356–365.

Tsuji, Y., Tanaka, T., Ishida, T., 1992. Lagrangian numerical simulation of plug flow of cohesionless particles in a horizontal pipe. Powder Technology 71 (3), 239–250.

Van Zeebroeck, M., Tijskens, E., Dintwa, E., Kafashan, J., Loodts, J., De Baerdemaeker, J., Ramon, H., 2006. The discrete element method (DEM) to simulate fruit impact damage during transport and handling: case study of vibration damage during apple bulk transport. Postharvest Biology Technology 41 (1), 92–100.

Van Liedekerke, P., Tijskens, E., Ramon, H., 2009. Discrete element simulations of the influence of fertiliser physical properties on the spread pattern from spinning disc spreaders. Biosystems Engineering 102 (4), 392–405.

Vansichen, R., De Baerdemaeker, J., 1991. Continuous wheat yield measurement on a combine. In: ASAE Symposium on Automated Agriculture for the 21st Century, Chicago. American Society of Agricultural Engineers, St. Joseph, Michigan, pp. 346–355.

Whitney, J.D., Ling, Q., Wheaton, T.A., Miller, W.M., 2001. A citrus harvesting labor tracking and yield mapping system. Applied Engineering Agriculture 17, 121–125.

Zijian, Z., Renwen, C., 2002. A new hysteresis compensation method for load cells. Transactions Nanjing University Aeronautics Astronautics 19, 89–93.